Journal of Membrane Science 384 (2011) 176–183

Contents lists available at SciVerse ScienceDirect

Journal of Membrane Science

journal homepage: www.elsevier.com/locate/memsci

Interaction of gas molecules with crystalline polymer separation membranes: Atomic-scale modeling and first-principles calculations

Yanting Wang[a,b], Sergey N. Rashkeev[a,*], John R. Klaehn[c], Christopher J. Orme[c], Eric S. Peterson[c]

[a] Center for Advanced Modeling and Simulation, Idaho National Laboratory, Idaho Falls, ID 83415-3553, USA
[b] Key Laboratory of Frontiers in Theoretical Physics, Institute of Theoretical Physics, Chinese Academy of Sciences, 55 Zhongguancun East Road, Beijing 100190, PR China
[c] Interfacial Chemistry, Idaho National Laboratory, Idaho Falls, ID 83415-2008, USA

ARTICLE INFO

Article history:
Received 9 March 2011
Received in revised form 3 September 2011
Accepted 13 September 2011
Available online 17 September 2011

Keywords:
Plasticization
Polybenzimidazole
Bis(isobutylcarboxy)polybenzimidazole
Kapton
Molecular dynamics (MD)

ABSTRACT

Carbon dioxide (CO_2)-induced plasticization can significantly decrease the gas separation performance of membranes in high-temperature or high pressure conditions, such as industrial methane (CH_4) separations. In this paper, we investigated the crystalline phase of three polymers (polybenzimidazole (PBI), bis(isobutylcarboxy)polybenzimidazole (PBI-Butyl), and Kapton™) and interactions between gas molecules (CO_2 and N_2) and these polymers. A novel, molecular dynamics (MD) based, computational technique was employed to find unknown crystalline structures of these polymer materials. The interaction of CO_2 and N_2 gases with these crystals was studied by first-principles calculations and by classical MD simulations. The results provide useful information for qualitative understanding the permeability, diffusivity, and plastic swelling in these materials caused by gas molecules absorbed in a polymer matrix.

1. Introduction

Carbon dioxide induced plasticization can significantly decrease the gas separation performance of membranes in high-temperature or high pressure conditions. For polymers employed as gas separation membranes, high permeability and high selectivity are essential for reducing capital and operating costs, respectively. Moreover, minimization of CO_2-induced plasticization is required for many new potential applications such as high temperature and/or high-pressure gas separations found in natural gas processing (CO_2/CH_4 separations), CO_2 separations for enhanced oil recovery, propylene/propane separations, butadiene/butane separations, and aromatic/aliphatic separations by pervaporation [1]. High performance polymers (glassy polymers), like polyimides and polybenzazoles (Kapton™ and polybenzimidazole) have excellent separation characteristics at low pressures for several gas pairs, but they cannot maintain this performance at high temperatures or pressures, especially in the presence of strong sorbing components (such as CO_2).

In high-pressure CO_2/CH_4 separations, problems arise due to CO_2 plasticization [2–6]. The polymer matrix is swollen by sorbing CO_2, which results in increasing CO_2 permeability. Simultaneously, the CH_4 permeability increases, therefore, the membrane loses its selectivity. When evaluating permeation vs. pressure curves for glassy polymers, the CO_2 permeability reaches equilibrium after long-term exposure; however, the selectivity does not improve. In membrane studies, plasticization is generally defined as an increase in the segmental motion of polymer chains, due to the presence of one or more sorbates, such that the permeability of both components increases and the selectivity decreases [2–5]. The loss in selectivity for CO_2/CH_4 and propylene/propane separations is mainly caused by a reduction in the diffusivity selectivity due to excessive segmental motion.

To make polymeric membranes attractive for natural gas sweetening and similar applications, CO_2 plasticization needs to be minimized. Over the past 25 years various schemes to reduce CO_2-induced plasticization have been studied, yet there are limited avenues to solve this problem. During this period, Idaho National Laboratory (INL) has investigated chemical modification of polymers, and an area of interest at INL has been with glassy polymers, polyimides and polybenzazoles. Long term experimental observation has shown that permeability and diffusivity of polymers determine the efficiency of gas separation, but theoretical studies at the molecular level are inadequate to interpret the connections between molecular structures of polymers and their gas-separation performance. In this paper we investigate some of these molecular level interactions by comparing molecular simulations with experimental data.

Glassy polymers that are used to generate gas separation membranes are known to form both crystalline and amorphous

* Corresponding author. Tel.: +1 208 526 9402; fax: +1 208 526 8254.
E-mail address: sergey.rashkeev@inl.gov (S.N. Rashkeev).

0376-7388/$ – see front matter © 2011 Elsevier B.V. All rights reserved.
doi:10.1016/j.memsci.2011.09.020

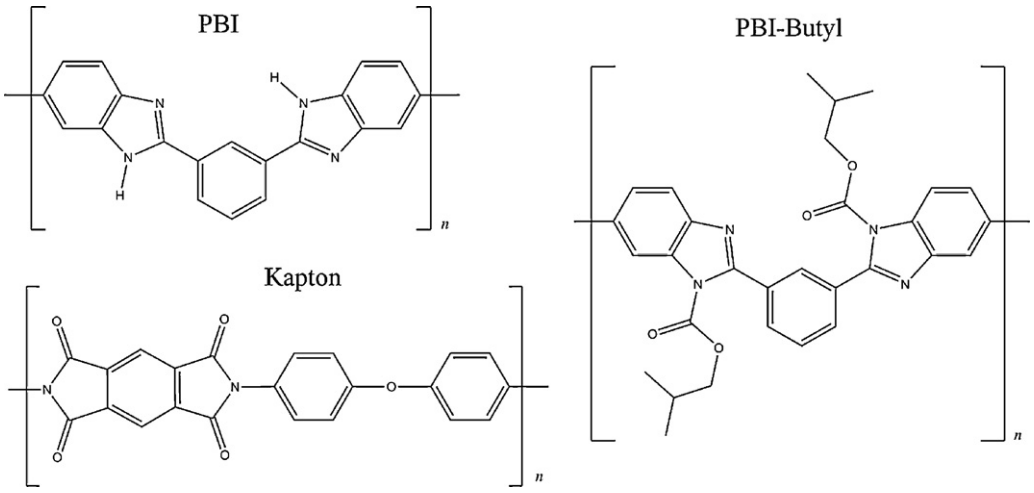

Fig. 1. Schematics of the molecular structure of PBI, PBI-Butyl, and Kapton.

regions. Since amorphous structures are statistically challenging to simulate and analyze, in this study, we only concentrate on the interactions of gas molecules with crystalline polymers. A novel computational technique has been employed to determine the crystalline structures of three polymers: polybenzimidazole (PBI), bis(isobutylcarboxy)polybenzimidazole (PBI-Butyl), and Kapton™. The interactions of CO_2 and N_2 gas molecules with those three crystals were studied by both first-principles calculations to investigate possible binding of gas molecules to the polymer matrix and calculating their migration barriers and transition states and by MD simulations to study the behavior and evolution of large ensembles of gas molecules within crystalline polymers. Our results suggest that CO_2 and N_2 molecules are physically but not chemically absorbed by the polymers, and the packing structure and interlayer coupling of polymer crystallites determine the permeability and diffusivity of gas molecules.

In particular, we found that crystalline PBI forms a very strong and closely packed structure, so that the diffusion barrier for gas molecules through the crystal layers is higher than the migration barrier parallel to the plane. The crystalline structure of PBI-Butyl is rigid, but larger interlayer distances due to the butyl side chains allow gas molecules to freely diffuse between layers. The Kapton crystalline structure is also closely packed, but the interlayer coupling is weaker than in PBI. As a consequence, gas molecules can be accommodated between layers which increases the interlayer distances and, therefore, increase the mobility of gas molecules. In general, the qualitative behavior for the diffusion of CO_2 and N_2 molecules is rather similar, even though there are changes in polymer structures due to the presence of these molecules. This work provides useful information on how the microscopic molecular structures determine the interactions of gas molecules with gas separation polymers.

2. Computational methods

In this study, the interactions of the PBI, PBI-Butyl, and Kapton crystals with two types of gas molecules, CO_2 and N_2, were investigated. For all-atom MD simulations, the empirical force parameters for CO_2 and N_2 were taken from Ref. [7]. The AMBER force field parameters for bonded interactions (bond lengths, bond and dihedral angles) and van der Waals (VDW) interactions [8] were used for modeling polymers at the atomistic level. Real polymers are made of long molecules with hundreds of repeating units, and current computer power is not sufficient to perform calculations for full-length polymer molecules at the atomistic level. To circumvent this problem, the end sites of model polymer chains were "connected" by applying periodic boundary condition (PBC) in one direction (X) in our simulations, and such infinite "periodic" molecules were used for simulating infinite polymer chains. The unit (single molecular) blocks for the PBI, PBI-Butyl, and Kapton polymers are shown in Fig. 1. For this article, we designate the single molecular unit structures as "single-unit" systems, while multi-molecular unit structures composed of repeating single molecular units are designated "chains".

To calculate the atomic partial charges, single-unit molecules were "saturated" by attaching one extra hydrogen atom at each connection site of the unit. Their geometries were optimized by the Gaussian 03 program [9] at the theoretical level of MP2/6-31g*. The RESP program [10] included in the AMBER software package was then employed to obtain the atomic partial charges by the standard two-step fitting procedure. The atomic partial charges in multi-unit polymer chains were assumed to be the same as those for single-unit molecules, with the extra hydrogen atoms removed and their partial atomic charges added to the adjacent connection sites. The partial charges were employed to calculate electrostatic interactions. The cutoff radius for VDW interaction is 10 Å, and that for the Coulomb interactions is 12 Å.

The MD simulations were performed by the LAMMPS simulation package [11] with a time step of 1 fs. The systems were coupled either to a Nosé–Hoover thermostat [12] for the constant *NVT* ensemble or to a Hoover barostat [13] for the constant *NPT* ensemble. The long-range electrostatic interactions were calculated using the Ewald summation process [14].

In general, it is quite difficult to determine the real structure of a crystal formed by long polymer molecules from experiment or computer simulations. To determine the most likely crystalline structures of the three polymers considered in this work, we developed a novel computational technique based on the MD simulations. First, 256 single-unit, hydrogen saturated, unconnected molecules of each polymer were positioned in a periodic three-dimensional lattice with large enough inter-molecular distances to avoid overlap between the molecules.

The system then went through a constant *NPT* all-atom MD simulation with temperature $T = 10$ K and pressure $P = 1$ atm for 100 ps. In such a relaxation scheme, single-unit molecular building blocks have enough freedom to adjust their orientation and finally form an energetically preferred crystalline structure. The lattice constants were then determined from the final equilibrated structures. The equilibrium was justified by the convergence of the system total energy. We assumed that the two connection points at both ends

Table 1
Lattice constants of the single-unit PBI, PBI-Butyl, and Kapton molecular systems.

Polymer	*XX* (Å)	*YY* (Å)	*ZZ* (Å)	*XY* (Å)	*XZ* (Å)	*YZ* (Å)
PBI	15.04	7.10	2.84	0.00	2.16	3.21
PBI-Butyl	15.61	12.29	3.53	5.49	3.92	8.89
Kapton	18.50	6.73	3.15	1.93	2.05	3.59

define the *X* direction and the backbone planar structures lie on the *XY* plane, i.e., the crystal unit vectors could be chosen in a quite general form **a** = (*XX*, 0, 0), **b** = (*XY*, *YY*, 0), **c** = (*XZ*, *YZ*, *ZZ*) (see Table 1). The mass densities corresponding to the relaxed PBI, PBI-Butyl, and Kapton structures are 1.489 g/cm^3, 1.130 g/cm^3, and 1.613 g/cm^3, respectively.

After this initial relaxation, all the single-unit molecules are still hydrogen saturated at both ends, i.e., they still do not form real multi-unit molecular polymer chains. To make a next step towards the structure of real polymers, we constructed small periodic systems with 1, 2, and 4 replicates (8-unit molecular systems) of the repeating units along the *X*, *Y*, and *Z* directions, respectively, using the above obtained lattice constants for each type of molecule. This time, the connection sites at the two ends of the *X*-oriented molecules were connected by a chemical bond with PBC, in order to mimic infinitely long polymer chains. These systems were also relaxed with all-atom *NPT* MD simulations at $T = 10$ K and $P = 1$ atm for 100 ps. This relaxation slightly adjusted positions of the atoms relatively to their initial positions in the single-unit systems. The average distances between polymer chains along the *Z* direction are listed in Table 2. They are noticeably larger than those for the single-unit systems considered above.

In addition to MD simulations, these 8-unit molecular systems were relaxed with first-principles calculations using the VASP codes [15,16]. The calculations were based on the density-functional-theory (DFT) with generalized gradient approximation (GGA) of PW-91 for exchange and correlation and plane waves [17,18]. Ultrasoft scalar relativistic pseudopotentials [19,20] and periodic supercells (with 288 atoms for PBI, 528 atoms for PBI-Butyl, and 312 atoms for Kapton) were used. The supercell is triclinic for PBI, and primitive orthorhombic for PBI-Butyl and Kapton. The point symmetry group for all the structures is trivial, i.e., it contains the identity operation only. The energy cutoff for the plane-wave basis was set at 400 eV, and all integrations over the Brillouin zone were done using the Monkhorst–Pack scheme with only one **k** point in the relevant irreducible wedge [21]. Inclusion of any additional **k** points was found to have minimal effect on the total-energy differences of interest here (which is not surprising for such large supercells). The structures were relaxed until the quantum-mechanical force on each atom in the supercell became smaller than 0.02 eV/Å. The average interlayer distances along the *Z* direction obtained from the first-principles calculations are also shown in Table 2.

For MD simulations of interactions between gas molecules and polymer crystalline structures at the room temperature, we used supercells with 5, 4, and 8 repeating units (160-unit molecular systems) along the *X*, *Y*, and *Z* directions, respectively. These supercells were constructed using the lattice constants calculated for the 8-molecule system, with a subsequent *NPT* MD relaxation at $T = 300$ K and $P = 1$ atm for 1 ns. The average distances between polymer chains in the *Z* direction in the relaxed configurations are slightly larger than those for small 8-unit systems simulated at $T = 10$ K because of larger thermal fluctuations of polymer chains at $T = 300$ K.

3. Results and discussion

In this section, we report the determined crystalline structures of polymers, as well as the results of first-principles calculations and classical MD simulations for gas molecules included in a polymer matrix. Our results suggest that CO_2 and N_2 molecules are physically but not chemically absorbed by the polymers, and the packing structure and interlayer coupling of polymer crystals determine the preferred migration direction of gas molecules.

3.1. Crystalline structures of polymers

Snapshots of equilibrated crystalline structures of the 160-unit molecular systems for PBI, PBI-Butyl, and Kapton are shown in Fig. 2. The obtained simulation box (a parallelepiped with PBCs applied in all of the three dimensions) sizes are shown in Table 3.

Both PBI and Kapton are closely packed structures because they consist of planar molecules, and the molecular layers can be positioned closely to each other. Also, due to their planar molecular structure, polymer chains in both systems exhibit a collective travelling wave motion along the *X* direction at $T = 300$ K. In contrast to these two systems, the interactions between butyl side chains of PBI-Butyl supporting the planar structures push the backbones further apart in both the *Y* and the *Z* directions. Therefore, the *Y* and *Z* equilibrium box sizes for PBI-Butyl are larger than those for PBI and Kapton. Also, the presence of side chains in the PBI-Butyl molecules significantly suppresses the collective travelling wave motion caused by thermal fluctuations.

3.2. First-principles calculations

As the crystalline structures of polymers were determined, first-principles calculations were employed to calculate the energy barrier for gas molecules migration in the directions parallel or perpendicular to the polymer layers. For each type of the three polymers, one CO_2 or NO_2 gas molecule was deposited between the layers of the 8-unit molecular system, as described in Section 2. The system (polymer crystal plus a gas molecule) was optimized with the VASP codes. The optimal migration paths and energy barriers for the migration of gas molecules in the directions parallel and perpendicular to the polymer layers were calculated using the nudged-elastic-band method [22].

The optimized structures of CO_2 and N_2 molecules in PBI are shown in Fig. 3. The top panels (cross section on *XZ* plane) show

Table 2
Average interlayer distances along the *Z* direction for crystalline PBI, PBI-Butyl, and Kapton determined for the single-unit molecular system, for the 8-unit molecular system from first-principles calculations, and for the 160-unit molecular system from classical MD simulations.

Polymer	Single-unit (Å)[a]	First-principle (Å)[b]	MD with PBC (Å)[c]	MD at 300 K (Å)[d]
PBI	2.84	3.26	3.11	3.23
PBI-Butyl	3.53	3.75	3.61	3.78
Kapton	3.15	3.47	3.36	3.38

[a] Single-unit: calculated for the system of 256 molecules; each of them consists of a single-unit molecule saturated by hydrogen atoms at both ends.
[b] First-principle: first-principles calculation results for 8-unit molecular systems with the special PBC applied along the *X* direction.
[c] MD with PBC: the same molecular structure as (b); simulated with classical MD at $T = 10$ K and $P = 1$ atm.
[d] MD at 300 K: the 160-unit molecular systems with the special PBC applied along the *X* direction simulated with classical MD at $T = 300$ K and $P = 1$ atm.

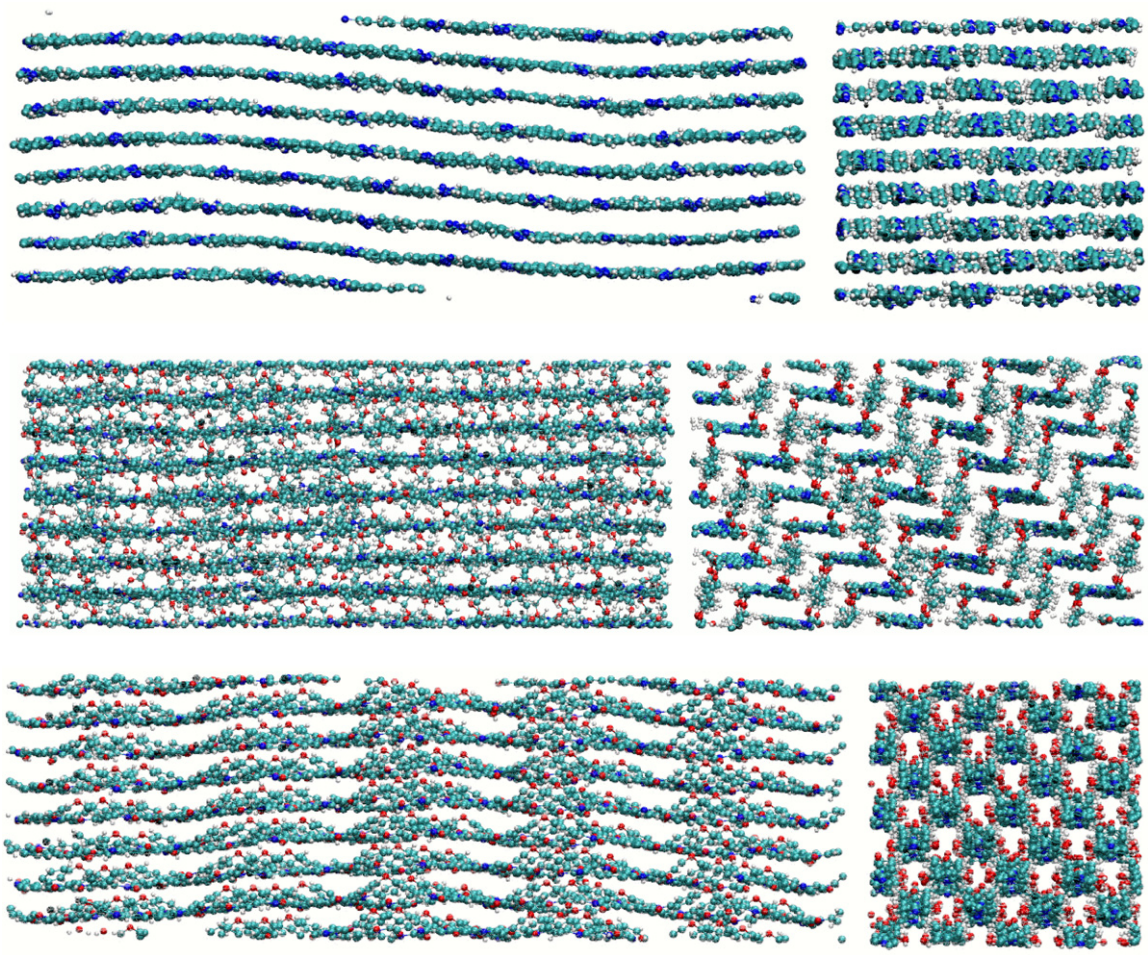

Fig. 2. Snapshots of crystalline PBI (top), PBI-Butyl (medium), and Kapton (bottom) at $T = 300$ K. The pictures on the left column show the *XZ* plane, and those on the right column show the *YZ* plane. Carbon atoms are shown in cyan, hydrogen – in white, nitrogen – in blue, oxygen – in red. (For interpretation of the references to color in this figure legend, the reader is referred to the web version of this article.)

that both CO_2 and N_2 molecules tend to be closer to one PBI layer along the *Z* direction rather than stay in the middle between two layers, while the bottom panels (cross section on *XY* plane) show that gas molecules are positioned between two PBI chains, indicating that gas molecules are physically but not chemically absorbed by the polymer. The minimum migration path of CO_2 parallel to the layers (shown by the dashed line) is positioned between the polymer chains. The migration path for N_2 is similar. The calculated migration energy barriers for the gas molecules parallel and perpendicular to the polymer layers are listed in the same figure. CO_2 has a smaller energy barrier (0.52 eV) than N_2 (0.71 eV) in the direction parallel to the polymer layers, but a larger barrier (1.40 eV) than N_2 (1.05 eV) when migrating perpendicular to the layers.

Fig. 4 shows the optimized structure of CO_2 inside PBI-Butyl. It can be seen that, although a CO_2 molecule is still physically attached to the polymer, the space between PBI-Butyl layers due to the side chains is large enough to easily accommodate the CO_2 molecule. Correspondingly, as listed in Table 4, the energy barriers for CO_2 to migrate parallel and perpendicular to PBI-Butyl layers have the same low value of 0.32 eV. The calculations of N_2 inside PBI-Butyl yielded similar results with even a lower energy barrier of 0.24 eV. These numbers indicate that CO_2 and N_2 molecules can easily move inside PBI-Butyl in any direction.

The optimized structure for a CO_2 molecule inside Kapton is shown in Fig. 5, and the energy barrier values for the CO_2 and N_2 migration between Kapton layers are listed in Table 4. Kapton, like PBI, also has a close-packed crystalline structure, but its

Table 3
The rectangular simulation box sizes for pure polymer crystals (160-unit molecular systems) and for polymer crystals with inserted gas molecules.

System	*X* (Å)	*Y* (Å)	*Z* (Å)	Volume (nm^3)
PBI	75.09 ± 0.11	28.38 ± 0.09	25.83 ± 0.12	55.05 ± 0.19
PBI + CO_2	75.08 ± 0.05	29.97 ± 0.11	25.82 ± 0.08	58.10 ± 0.17
PBI + N_2	75.09 ± 0.06	29.57 ± 0.18	26.03 ± 0.10	57.68 ± 0.17
PBI-Butyl	75.55 ± 0.05	52.35 ± 0.18	30.25 ± 0.07	119.51 ± 0.31
PBI-Butyl + CO_2	75.52 ± 0.05	52.05 ± 0.20	30.30 ± 0.08	119.08 ± 0.39
PBI-Butyl + N_2	75.52 ± 0.05	52.41 ± 0.20	30.22 ± 0.08	119.61 ± 0.37
Kapton	84.77 ± 0.10	27.50 ± 0.04	27.02 ± 0.07	62.97 ± 0.15
Kapton + CO_2	84.91 ± 0.06	27.80 ± 0.09	28.36 ± 0.10	66.94 ± 0.16
Kapton + N_2	84.65 ± 0.08	26.63 ± 0.11	30.43 ± 0.14	68.58 ± 0.18

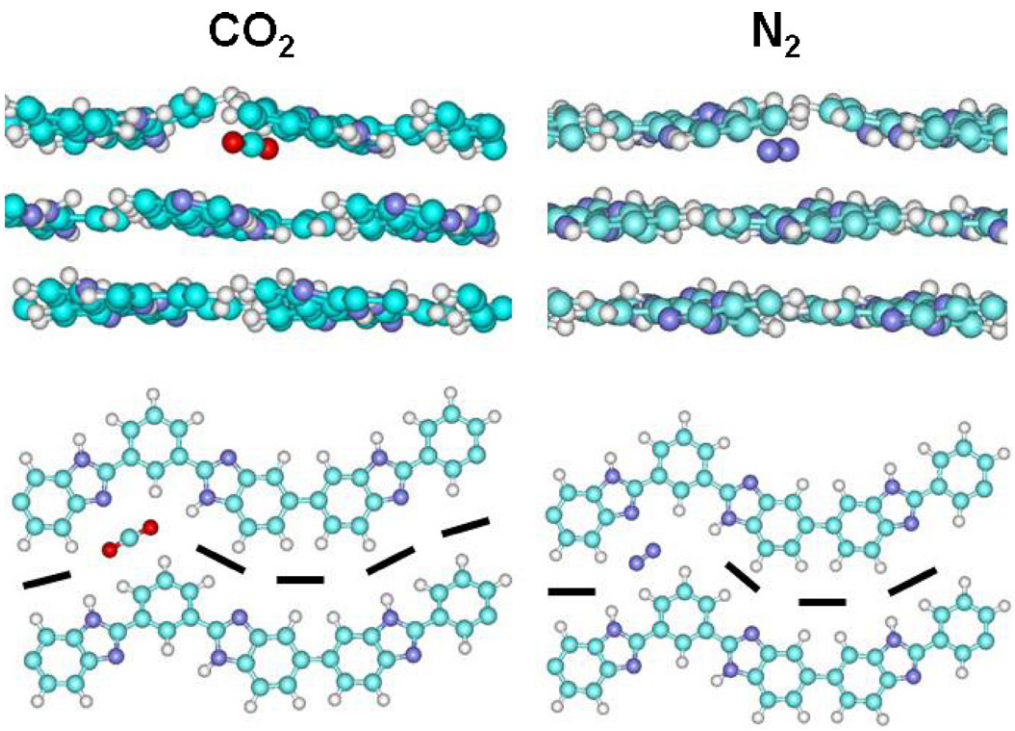

Fig. 3. Optimized structures of CO_2 (left column) and N_2 (right column) molecules between PBI layers and the migration path (illustrated by dashed line) of CO_2 parallel to the layers by first-principles calculations. The top panels are cross-sections along the *XZ* plane and the bottom panels are along the *XY* plane. Carbon atoms are shown in cyan, hydrogen – in white, nitrogen – in blue. The trajectories of the migration in the *XY* plane and the orientation of the molecular axis at different points of the path are indicated by dashed black lines. (For interpretation of the references to color in this figure legend, the reader is referred to the web version of this article.)

Table 4
Comparison of the energy barriers for CO_2 and N_2 in the directions parallel and perpendicular to polymer layers.

Polymer	CO_2 barrier parallel (eV)	N_2 barrier parallel (eV)	CO_2 barrier perpendicular (eV)	N_2 barrier perpendicular (eV)
PBI	0.52	0.71	1.40	1.05
PBI-Butyl	0.32	0.24	0.32	0.24
Kapton	0.48	0.50	0.80	0.85

interlayer interactions are softer than those in PBI. Therefore, all the energy barriers for the migration parallel to the layers are lower than those in PBI, although the anisotropy of the migration barriers (perpendicular and parallel to the layers) is still high.

In these calculations we did not observe any significant interaction between a CO_2 (N_2) molecule introduced in polymer and individual atomic sites of the polymer network with a formation of low-energy bound states. The strongest bonding we observed, was the formation of weak bond (0.35 eV) between O atom of CO_2 molecule and hydrogen unsaturated N atoms of the PBI and PBI-Butyl polymer networks (such type of sites is absent in Kapton).

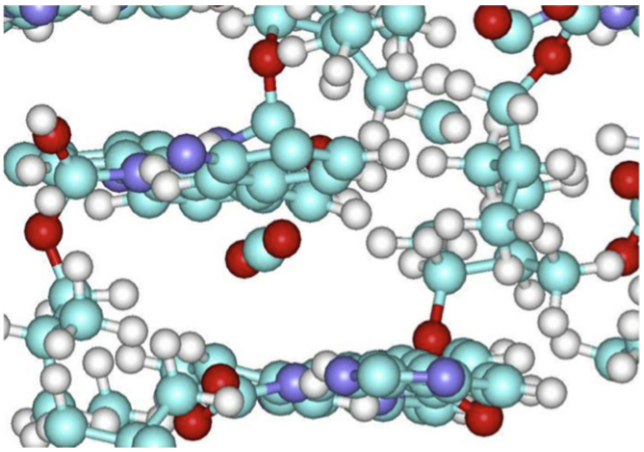

Fig. 4. Optimized structure of a CO_2 molecule between PBI-Butyl layers by first-principles calculations. C atoms are shown in cyan, H – in white, N – in blue, O – in red. (For interpretation of the references to color in this figure legend, the reader is referred to the web version of this article.)

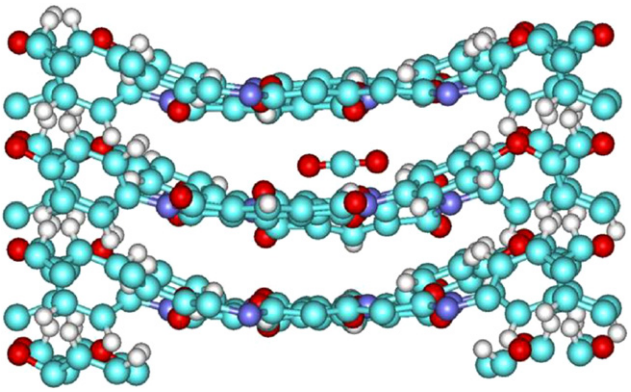

Fig. 5. Optimized structure of CO_2 between Kapton layers by first-principles calculations. C atoms are shown in cyan, H – in white, N – in blue, O – in red. (For interpretation of the references to color in this figure legend, the reader is referred to the web version of this article.)

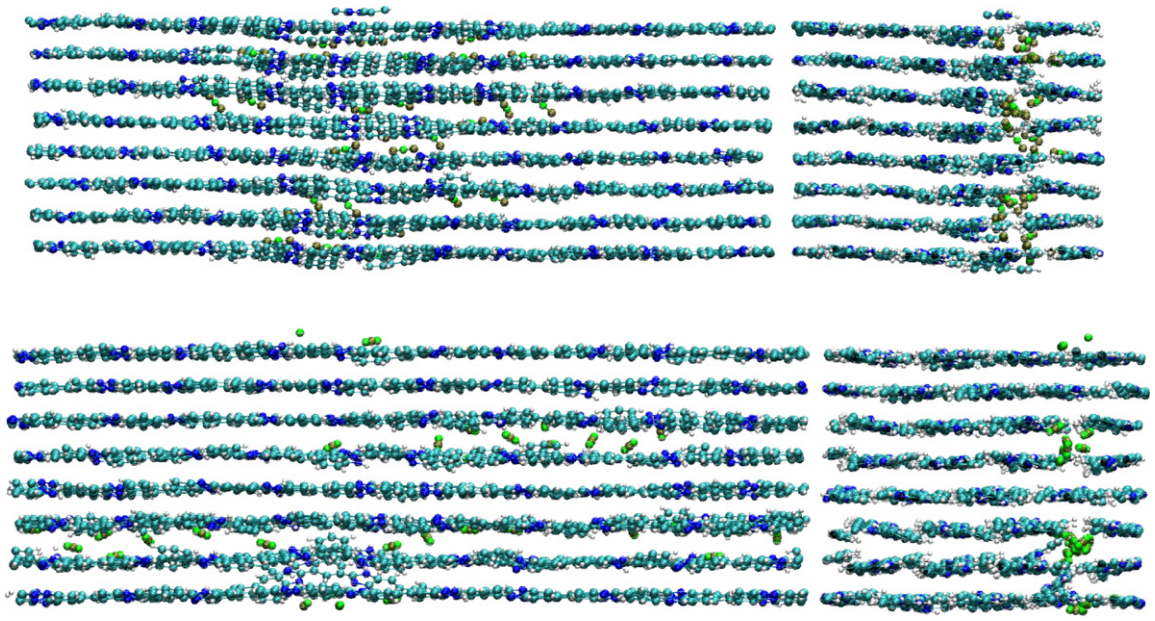

Fig. 6. Snapshots of crystalline PBI interacting with CO_2 (top) and N_2 (bottom) gas at $T = 300$ K and $P = 1$ atm. The pictures on the left column show the *XZ* plane, and those on the right column show the *YZ* plane. Carbon atoms are shown in cyan, hydrogen – in white, nitrogen – in blue, and oxygen – in red. The gas molecules are drawn in other colors. (For interpretation of the references to color in this figure legend, the reader is referred to the web version of this article.)

However, this bonding forms a local energy minimum only while the absolute energy minimum is still defined by the optimized structures described above.

3.3. Classical MD simulations

To investigate how massive clusters of gas molecules could affect crystalline polymer structures, we inserted clusters of 32 CO_2 or 32 N_2 molecules inside the 160-unit molecular polymer supercell (which corresponds to the concentration of gas molecules of about 1 mol/L). The centers of the inserted molecules were initially positioned in a plane Y = const while their X and Z coordinates varied, and the PBCs were then reapplied to the whole polymer crystal + gas systems. These new structures were then re-equilibrated with a constant *NPT* MD simulation at $T = 300$ K and $P = 1$ atm for 1 ns, followed by another 1 ns *NPT* run for sampling. The data were evenly sampled every 1 ps. In the equilibration process, the gas molecules were pushed to diffuse into the spaces between polymer layers.

The final equilibrated configurations of CO_2 and N_2 clusters in PBI matrix are shown in Fig. 6. It can be seen that in spite of the gas molecules being embedded between PBI layers, the PBI crystal structure itself did not undergo any significant changes, as compared with the structure shown in Fig. 2. The only exception is the fact that the presence of gas molecules significantly suppressed the collective wave motion of the crystal layers. The average sizes of boxes corresponding to the PBI + gas systems were calculated

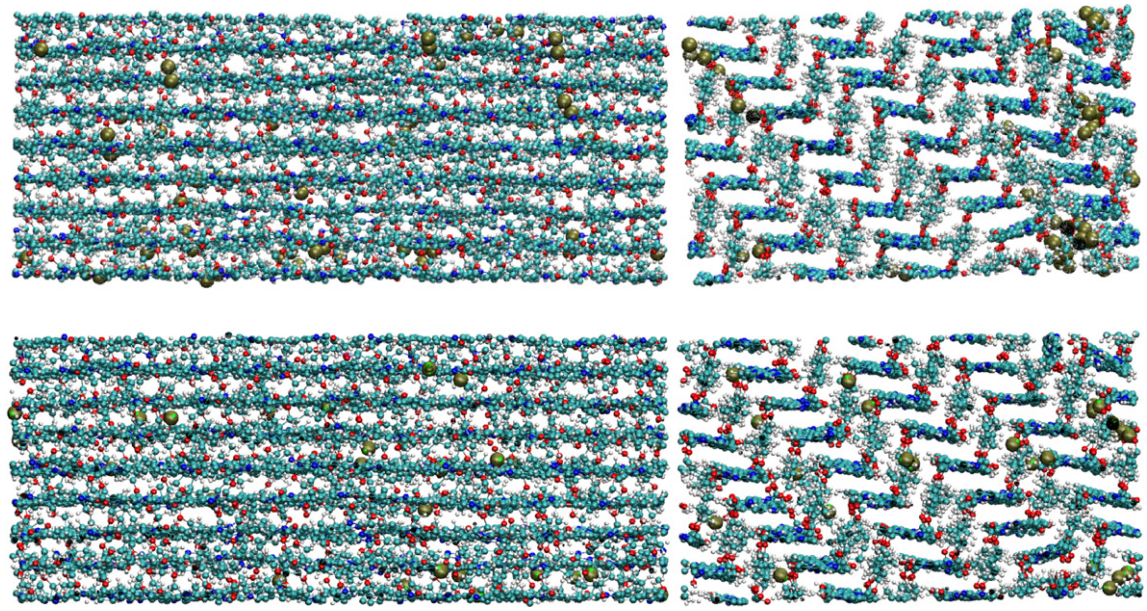

Fig. 7. Snapshots of crystalline PBI-Butyl interacting with CO_2 (top) and N_2 (bottom) at $T = 300$ K and $P = 1$ atm. The pictures on the left column show the *XZ* plane, and those on the right column show the *YZ* plane. Carbon atoms are shown in cyan, hydrogen – in white, nitrogen – in blue, and oxygen – in red. Inserted gas molecules are shown in larger dark gold spheres. (For interpretation of the references to color in this figure legend, the reader is referred to the web version of this article.)

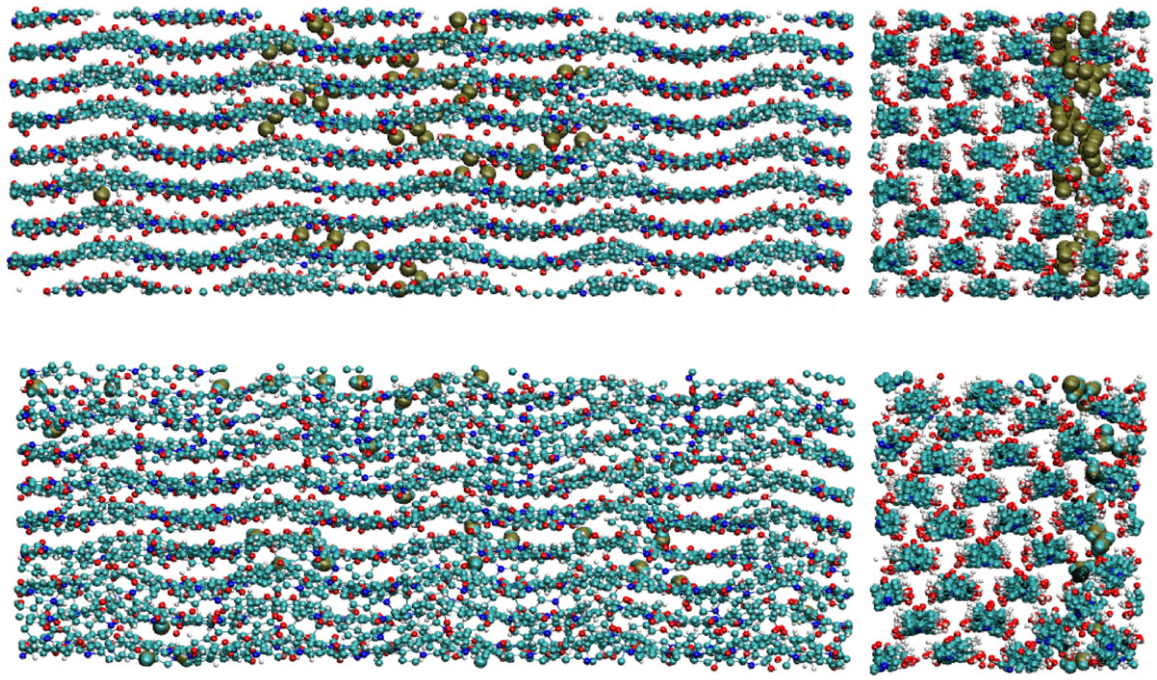

Fig. 8. Snapshots of crystalline Kapton interacting with CO_2 (top) and N_2 (bottom) at $T = 300$ K and $P = 1$ atm. The pictures on the left column show the *XZ* plane, and those on the right column show the *YZ* plane. Carbon atoms are shown in cyan, hydrogen – in white, nitrogen – in blue, and oxygen – in red. Inserted gas molecules are shown in larger dark gold spheres. Carbon atoms are shown in cyan, hydrogen – in white, nitrogen – in blue. The trajectories of the migration in the XY plane and the orientation of the molecular axis at different points of the path are indicated by dashed black lines. (For interpretation of the references to color in this figure legend, the reader is referred to the web version of this article.)

from the sampled data and listed in Table 3. Comparing with those for the pure PBI crystal system, we notice that the presence of gas molecules practically does not change the size of the box in the *Z* direction (the change is below 1%), but increases the size of the box in the *Y* direction by about 5.6% for CO_2 and 4.2% for N_2 (see Table 3 and Fig. 6). The crystal cell volume increases due to its dimensional increase in the *Y* direction. Such a behavior is consistent with first-principles calculations which show that both CO_2 and N_2 always prefer to stay close to one PBI layer rather than to go into interstitial space between two layers because the interlayer coupling in a close-packed PBI crystal is quite strong, i.e., the interlayer interstitial space is limited (Fig. 3). At the same time, gas molecules make the nearest polymer layer to swell in the lateral (*Y*) direction by pushing the neighboring polymer chains apart from each other. Consequently, the presence of gas molecules increases the crystal cell size in the *Y* direction but not in the *Z* direction. An interesting result is that both CO_2 and N_2 clusters in PBI crystal behave in a similar manner. The migration of gas molecules mainly occurs in the direction parallel to the layers, and CO_2 molecules exhibit higher mobility than N_2 molecules.

Because the butyl side chain of PBI-Butyl molecule significantly increase the spaces between polymer chains both in the *Y* and in the *Z* directions, the gas molecules are easily accommodated in the spaces between polymer chains, as illustrated in Fig. 7. The gas molecules diffuse into the PBI-Butyl crystal, and may temporarily stay in the interstitial space between side chains (gas molecules are still very mobile and may migrate within the crystal). The data in Table 3 indicates that the presence of gas molecules does not change the lattice parameters and total volumes of the PBI-Butyl crystal cell, i.e., the swelling effects caused by gas molecules in PBI-Butyl crystal are much weaker in nature than those in PBI.

The data in Table 3 also show that CO_2 molecules increase the spacing between polymer chains in the *Z* direction of the Kapton crystal cell while there is no swelling in the *Y* direction, but the presence of N_2 molecular clusters increases the box size in the *Z* direction and decreases it in the *Y* direction. The snapshots in Fig. 8 demonstrate that, because the intermolecular attractions between Kapton layers are relatively weak and the presence of joint oxygen atom connecting two rings (Fig. 1) increases the flexibility of Kapton, both gas molecules (CO_2 and N_2) can penetrate into the polymer chains, and the planar structure of the polymers tilts to accommodate the gas molecules. N_2 molecules distort the Kapton crystal structure to a higher degree than CO_2 molecules.

4. Conclusions

We developed a novel computational technique that employs MD simulations together with first-principles, atomic-scale calculations to determine crystalline structures of polymers. We found that PBI forms a close-packed crystal structure, and its strength is related to the all-ring, planar molecular structure. The crystal structure of the PBI-Butyl polymer is rigid but the interlayer distance is much larger than in PBI because of the presence of butyl side chains. Kapton also crystallizes in a close-packed structure, but its strength is lower than the strength of the PBI crystal structure due to flexibility of its molecule because of the presence of joint oxygen atom connecting two rings.

The mechanical properties of the polymer crystals which are determined by their molecular structures directly affect the interaction between gas molecules and the crystal. First-principles calculations indicate that CO_2 and N_2 molecules have a higher migrating energy barrier in the direction perpendicular to the PBI polymer layers, which is consistent with the close-packed molecular structure and strong intermolecular attraction in this material. Correspondingly, MD simulations demonstrate that CO_2 and N_2 molecules can hardly penetrate into the PBI layers. On the other hand, large spaces between PBI-Butyl layers due to the presence of the butyl side chains allow CO_2 and N_2 molecules to be easily accommodated into the crystal without any significant deformation of the crystalline structure, and these molecules are free to

migrate, as indicated by both the first-principles calculations and the MD simulations. The close-packed structure of Kapton also results in a higher migrating energy barrier to gas molecule migration in the direction perpendicular to the polymer layers, but the flexibility of Kapton molecules results in smaller energy barrier values than in PBI which allows gas molecules to penetrate into the layers. First-principles calculations also show that CO_2 and N_2 molecules are physically (but not chemically) absorbed by all of the three considered polymer crystals.

This work demonstrates how the microscopic molecular structure determines the interactions of gas molecules with polymer crystals. However, in experiments and real life industrial applications glassy polymers used as gas separation membranes always contain both crystalline and amorphous regions. Therefore, results of this work are still insufficient to establish one-to-one correspondence between calculations and experiments. Further theoretical studies should also include amorphous regions of polymers, in order to better understand the permeability and diffusivity of gas molecules in polymer membranes. This work, however, provides useful information on how microscopic molecular structures determine the interactions of gas molecules with gas separation polymers and on understanding the relation between diffusivity and permeability of polymer membranes, as well as the plastic swelling in these materials caused by gas molecules absorbed in a polymer matrix.

Acknowledgments

We would like to acknowledge the INL Laboratory Directed Research and Development (LDRD) program and the U.S. Department of Energy, Office of Nuclear Energy for financial support. This research was also supported in part by a Grant of computer time from High Performance Computer Center at Idaho National Laboratory. This manuscript has been authored by Battelle Energy Alliance, LLC under Contract No. DE-AC07-05ID14517 with the U.S. Department of Energy. Also, this research used resources of the NERSC, which is supported in part by the U.S. DOE under Contract No. DE-AC02-05CH11231. Yanting Wang was also partially supported by the Hundred Talent Program of the Chinese Academy of Sciences. The United States Government retains and the publisher, by accepting the article for publication, acknowledges that the United States Government retains a nonexclusive, paid-up, irrevocable, world-wide license to publish or reproduce the published form of this manuscript, or allow others to do so, for United States Government purposes.

References

[1] D. Katarzynski, F. Pithan, C. Staudt, Pervaporation of milti-component aromatic/aliphatic mixtures through copolyimide membranes, Sep. Sci. Technol. 43 (2008) 59–70.
[2] E.S. Sanders, Penetrant-induced plasticization and gas permeation in glassy polymers, J. Membr. Sci. 37 (1988) 63–80.
[3] A.R. Berens, H.B. Hopfenberg, Induction and measurement of glassy-state relaxations by vapor sorption techniques, J. Polym. Sci.: Polym. Phys. Ed. 17 (1979) 1757–1770.
[4] W.J. Koros, A.H. Chan, D.R. Paul, Sorption and transport of various gases in polycarbonate, J. Membr. Sci. 2 (1977) 165–190.
[5] R.T. Chern, W.J. Koros, E.S. Sanders, R. Yui, Second component effects in sorption and permeation of gases in glassy polymers, J. Membr. Sci. 15 (1983) 157–169.
[6] G.K. Fleming, S.M. Jordan, W.J. Koros, Processes to condition gas permeable membranes, U.S. Patent 4,755,192 (July 5, 1988).
[7] J.J. Potoff, J.I. Siepmann, Vapor–liquid equilibria of mixtures containing alkanes, carbon dioxide, and nitrogen, AIChE J. 47 (2001) 1676–1682.
[8] W.D. Cornell, P. Cieplak, C.I. Bayly, I.R. Gould, K.M. Merz Jr., D.M. Ferguson, D.C. Spellmeyer, T. Fox, J.W. Caldwell, P.A. Kollman, A second generation force field for the simulation of proteins, nucleic acids, and organic molecules, J. Am. Chem. Soc. 117 (1995) 5179–5197.
[9] M.J. Frisch, G.W. Trucks, H.B. Schlegel, G.E. Scuseria, M.A. Robb, J.R. Cheeseman, J.A. Montgomery Jr., T. Vreven, K.N. Kudin, J.C. Burant, J.M. Millam, S.S. Iyengar, J. Tomasi, V. Barone, B. Mennucci, M. Cossi, G. Scalmani, N. Rega, G.A. Petersson, H. Nakatsuji, M. Hada, M. Ehara, K. Toyota, R. Fukuda, J. Hasegawa, M. Ishida, T. Nakajima, Y. Honda, O. Kitao, H. Nakai, M. Klene, X. Li, J.E. Knox, H.P. Hratchian, J.B. Cross, V. Bakken, C. Adamo, J. Jaramillo, R. Gomperts, R.E. Stratmann, O. Yazyev, A.J. Austin, R. Cammi, C. Pomelli, J.W. Ochterski, P.Y. Ayala, K. Morokuma, G.A. Voth, P. Salvador, J.J. Dannenberg, V.G. Zakrzewski, S. Dapprich, A.D. Daniels, M.C. Strain, O. Farkas, D.K. Malick, A.D. Rabuck, K. Raghavachari, J.B. Foresman, J.V. Ortiz, Q. Cui, A.G. Baboul, S. Clifford, J. Cioslowski, B.B. Stefanov, G. Liu, A. Liashenko, P. Piskorz, I. Komaromi, R.L. Martin, D.J. Fox, T. Keith, M.A. Al-Laham, C.Y. Peng, A. Nanayakkara, M. Challacombe, P.M.W. Gill, B. Johnson, W. Chen, M.W. Wong, C. Gonzalez, J.A. Pople, Gaussian 03, Revision C.02, Gaussian, Inc., Wallingford, CT, 2004.
[10] C.I. Bayly, P. Cieplak, W. Cornell, P.A. Kollman, A well-behaved electrostatic potential based method using charge restraints for deriving atopic charges: the RESP model, J. Phys. Chem. 97 (1993) 10269–10280.
[11] S.J. Plimpton, Fast parallel algorithms for short-range molecular dynamics, J. Comp. Phys. 117 (1995) 1–19, Also: http://lammps.sandia.gov.
[12] W.G. Hoover, Canonical dynamics: equilibrium phase-space distributions, Phys. Rev. A 31 (1985) 1695–1697.
[13] S. Melchionna, G. Ciccotti, B.L. Holian, Hoover NPT dynamics for systems varying in shape and size, Mol. Phys. 78 (1993) 533–544.
[14] M.P. Allen, D.J. Tildesley, Computer Simulation of Liquids, Clarendon Press, Oxford, 1987.
[15] G. Kresse, J. Furthmüller, Efficient iterative schemes for *ab initio* total-energy calculations using a plane-wave basis set, Phys. Rev. B 54 (1996) 11169–11186.
[16] G. Kresse, J. Hafner, *Ab initio* molecular dynamics for open-shell transition metals, Phys. Rev. B 48 (1993) 13115–13118.
[17] J.P. Perdew, J.A. Chevary, S.H. Vosko, K.A. Jackson, M.R. Pederson, D.J. Singh, C. Fiolhais, Atoms, molecules, solids, and surfaces: applications of the generalized gradient approximation for exchange and correlation, Phys. Rev. B 46 (1992) 6671–6687.
[18] J.P. Perdew, J.A. Chevary, S.H. Vosko, K.A. Jackson, M.R. Pederson, D.J. Singh, C. Fiolhais, Erratum: atoms, molecules, solids, and surfaces: applications of the generalized gradient approximation for exchange and correlation, Phys. Rev. B 48 (1993) 4978.
[19] G. Kresse, J. Hafner, Norm-conserving and ultrasoft pseudopotentials for first-row and transition elements, J. Phys.: Condens. Matter 6 (1994) 8245–8257.
[20] D. Vanderbilt, Soft self-consistent pseudoponentials in a generalized eigenvalue formalism, Phys. Rev. B 41 (1990) 7892–7895.
[21] D.J. Chadi, M.L. Cohen, Special points in the Brillouin zone, Phys. Rev. B 8 (1973) 5747–5753.
[22] H. Jonsson, G. Mills, K.W. Jacobsen, Nudged elastic band method for finding minimum energy paths of transitions, in: B.J. Berne, G. Ciccotti, D.F. Coker (Eds.), Classical and Quantum Dynamics in Condensed Phase Simulations, World Scientific, River Edge, NJ, 1998, p. 385.